coatings

MDPI

Article

Numerical Study on Composite Multilayer Insulation Material for Liquid Hydrogen Storage

Yi Ding [1,2], Dongliang Shao [1,2], Suke Jin [1,2], Meng Yu [1,2], Yubo Wang [3] and Long Jiang [4,*]

[1] Special Equipment Safety Supervision Inspection Institute of Jiangsu Province, Nanjing 210036, China; 11627057@zju.edu.cn (D.S.)
[2] Key Laboratory of Liquid Hydrogen Energy Storage and Transportation Equipment for Jiangsu Province Market Regulation, Nanjing 210036, China
[3] School of Energy, Changzhou University, Changzhou 213164, China
[4] Institute of Refrigeration and Cryogenics, Zhejiang University, Hangzhou 310027, China
* Correspondence: jianglong@zju.edu.cn

Abstract: This study investigated the heat transfer characteristics of composite multilayer insulation (MLI) materials used for the storage and transport of liquid hydrogen at cryogenic temperatures. This research focused on analyzing the effects of thermal boundary temperature, total layer count, and vacuum level on the heat flux through the insulation material. Based on the layer-by-layer model, a heat transfer model of composite MLI was constructed. This research introduces a novel method for analyzing the heat transfer properties of composite MLI in the liquid hydrogen temperature range. Results indicate that heat flux increases with higher thermal boundary temperatures, with the MLI layers near the cold boundary playing a critical role in overall insulation performance. Additionally, numerical analysis was conducted to examine the impact of different material combinations and variations in vacuum level on heat transfer characteristics. Findings reveal that adding spray-on foam insulation reduces heat flux by 20.76% compared to using MLI alone. Furthermore, increasing the total number of MLI layers effectively mitigates heat flux increase, achieving an optimal heat flux of 0.5377 W/m^2 with a total of 50 layers.

Keywords: composite multilayer insulation; liquid hydrogen temperature range; heat transfer characteristics; heat flux

Citation: Ding, Y.; Shao, D.; Jin, S.; Yu, M.; Wang, Y.; Jiang, L. Numerical Study on Composite Multilayer Insulation Material for Liquid Hydrogen Storage. *Coatings* **2024**, *14*, 1417. https://doi.org/10.3390/coatings14111417

Academic Editor: Gianfranco Carotenuto

Received: 5 October 2024
Revised: 30 October 2024
Accepted: 6 November 2024
Published: 8 November 2024

1. Introduction

Liquid hydrogen technology serves as a critical method for hydrogen energy applications and large-scale storage and transportation, offering advantages such as high volumetric hydrogen storage density and purity. It has already been applied in various fields, including chemical engineering and steel refining [1,2]. However, due to its low liquefaction temperature and latent heat of vaporization [3], it is highly susceptible to cold losses during storage and transport [4,5]. To minimize the loss of liquid hydrogen, effective insulation methods must be carefully chosen.

Literature research indicates that using composite multilayer insulation materials can significantly reduce evaporative losses of low-temperature liquids. The predominant configuration of composite multilayer insulation is comprised of SOFI and MLI [6], and SOFI is primarily utilized for thermal leak protection of low-temperature tanks at ambient pressure. MLI consists of alternating high-reflectivity radiation layers and low thermal conductivity spacer layers, which utilize successive layer reflections to achieve high thermal resistance against radiative heat, thereby reducing tank heat leakage [7].

Extensive theoretical and experimental research has been conducted on the thermal insulation performance and structural optimization of composite multilayer insulation materials both domestically and internationally. Hastings et al. [8] conducted experimental

studies on 3.53 mm SOFI and 45-layer variable-density MLI in the liquid nitrogen temperature range, achieving a heat leakage of 0.31 W/m^2 for the composite MLI. Huang et al. [9] developed a numerical model based on the finite volume method, considering radiation and thermal conduction effects. The model computed an effective thermal conductivity with less than 4% deviation from measured values. Li et al. [10] established a layer-by-layer model to evaluate MLI performance, demonstrating that 50 layers provide optimal thermal insulation, with a vacuum level below 0.01 Pa. Maynard et al. [11] primarily discussed the influence of hydrogen and nitrogen as residual gases in a degraded cold vacuum, leading to transient and complex interactions in achieving a steady-state condition. Jiang et al. [12] investigated the relationship between environmental humidity and composite MLI in the liquid nitrogen temperature range through theoretical and experimental studies, revealing an approximate 13.07% increase in apparent thermal conductivity with rising humidity. Hastings et al. [13] conducted experimental studies using a versatile hydrogen test bed, measuring a heat flux of 0.22 W/m^2 into a liquid hydrogen tank under high vacuum conditions at an ambient temperature of 305 K. Additionally, other researchers [14–19] studied the heat transfer behavior of composite MLI and variations in insulation performance related to environmental pressure, spacer materials, radiation shield emissivity, ratio of entropy generation, layer density, or specific form of cryogenic vessel in the liquid nitrogen or hydrogen temperature range.

Nevertheless, existing studies primarily focus on the insulation performance of MLI under liquid nitrogen temperature conditions, on typical MLI heat transfer models within the hydrogen temperature range, or a cryogenic vessel with a vapor-cooled shield. The thermal characteristics and temperature distribution of composite MLI in the liquid hydrogen temperature range, however, remain unclear. Considering the different storage media that can lead to changes in internal temperature distribution and thermal properties of MLI, resulting in varied heat transfer characteristics within the materials, a numerical model predicting the interlayer temperature distribution of composite MLI in the liquid hydrogen temperature range based on the layer-by-layer model is proposed and validated for accuracy. Subsequently, the combined effects of MLI and foam insulation materials on heat transfer in liquid hydrogen tanks are analyzed. This study explored the evolution of heat flux with thermal boundary temperature, vacuum degree, and number of layers for composite multilayer materials in the liquid hydrogen temperature range, thereby providing a theoretical foundation for the widespread application of composite MLI in liquid hydrogen storage tanks.

2. Methodology

A numerical model was developed to study the interlayer temperature distribution of composite MLI within the liquid hydrogen temperature range, as illustrated in Figure 1. The SOFI used is a polyurethane foam coating, while the multilayer material consists primarily of radiation layers consisting of aluminized films and spacer layers made of polyester. Considering that the heat transfer in composite materials involves multiple modes—including radiation, conduction, and convection—that interact with each other, the actual situation is quite complex. To ensure computational accuracy, the following assumptions are constructed [20]:

(1) The surrounding environmental temperature and vacuum degree around the composite MLI are constant.
(2) The space between adjacent radiation screens within the multilayer materials is finite and enclosed.
(3) Longitudinal heat transfer within the materials is negligible, and all heat transfer is assumed to be axial.
(4) The contact thermal resistance between SOFI and MLI under steady conditions is neglected.

Thus, heat transfer through the composite MLI can be considered one-dimensional. Since all heat transfer occurs axially, the total heat flux through the composite MLI aligns

with the heat flux through both the MLI and SOFI layers. As shown in Figure 1, the cold boundary is the interface where the SOFI contacts the outer wall of the inner vessel, while the hot boundary is the interface where the MLI contacts the inner wall of the vacuum jacket of the cryogenic vessel, which can be expressed as follows:

$$q_{\mathrm{SOFI}} = q_{\mathrm{MLI}} = q_{\mathrm{tot}} \tag{1}$$

where q_{tot} represents total heat flux through the composite MLI ($\mathrm{W/m^2}$), q_{MLI} denotes heat flux through the MLI ($\mathrm{W/m^2}$), and q_{SOFI} indicates heat flux through the SOFI ($\mathrm{W/m^2}$).

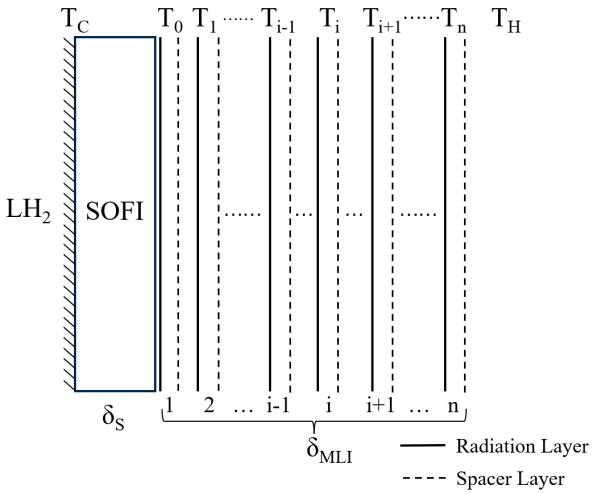

Figure 1. The schematic diagram of the numerical model.

2.1. Heat Transfer in SOFI

The heat flux through the SOFI (q_{SOFI}) can be expressed using Fourier's law:

$$q_{\mathrm{SOFI}} = \frac{\lambda_{\mathrm{SOFI}}}{L}(T_0 - T_{\mathrm{C}}) \tag{2}$$

where λ_{SOFI} is a temperature-dependent function, obtained by Barrios et al. [21] through fitting experimental data:

$$\lambda_{\mathrm{SOFI}} = 4 \times 10^{-9} T_{\mathrm{S}}^3 - 2 \times 10^{-6} T_{\mathrm{S}}^2 - 0.009 \tag{3}$$

where L is thickness of the SOFI in the composite MLI (m), T_{C} is cold boundary temperature of the composite MLI (K), T_0 is interlayer temperature between the SOFI and MLI (K), and T_{S} is internal temperature of the SOFI (K).

2.2. Heat Transfer in MLI

The heat transfer mechanisms in MLI are primarily related to the application environment. Total heat transfer includes radiative heat transfer, gaseous conduction, solid conduction, and convective heat transfer. Given the small spacing between adjacent radiation and spacer layers, convective heat transfer is generally assumed to be non-existent in MLI [22]. Therefore, the heat leakage in MLI primarily includes radiative heat transfer q_{r}, gaseous conduction q_{g}, and solid conduction q_{s}, which can be expressed as follows:

$$q_{\mathrm{MLI}} = q_{\mathrm{r}} + q_{\mathrm{g}} + q_{\mathrm{s}} \tag{4}$$

The gaseous conduction in MLI (q_{g}) is given by the following:

$$q_{\mathrm{g}} = \frac{\gamma + 1}{\gamma - 1}\left(\frac{R}{8\pi MT}\right)^{\frac{1}{2}} P\alpha(T_{\mathrm{i}} - T_{\mathrm{i-1}}) \tag{5}$$

where α is thermal accommodation coefficient (0.9 for gases), P is vacuum degree (Pa), T_i and T_{i-1} are the temperatures at the two ends of node layer i, γ is the ratio of C_p and C_v, C_p is specific heat at constant pressure, C_v is specific heat at constant volume, and R is universal gas constant, valued at 8.315 kJ/(mol·K).

The solid conduction in MLI (q_s) is given by the following:

$$q_s = \frac{C_2 f \lambda}{\delta}(T_i - T_{i-1}) \tag{6}$$

where C_2 is an empirical parameter (0.008), δ is thickness of the spacer layer (m), and f is the relative density of the spacer layer compared to the MLI (0.02). For polyester spacers, λ is a function of T_i and T_{i-1} as described by the following [13]:

$$\lambda = 0.017 + 7 \times 10^{-6} \times (800 - \frac{(T_i + T_{i-1})}{2}) + 0.0228 \times \ln(\frac{T_i + T_{i-1}}{2}) \tag{7}$$

The radiative heat transfer in MLI (q_r) is given by the following:

$$q_r = \frac{\sigma(T_i^4 - T_{i-1}^4)}{(\frac{1}{\varepsilon_i} + \frac{1}{\varepsilon_{i-1}} - 1)} \tag{8}$$

where σ is the Stefan–Boltzmann constant (5.67×10^{-8} W/m^2·K^4), T_i and T_{i-1} are the temperatures at the two ends of node layer i, and ε_i and ε_{i-1} are the emissivities of the hot and cold surfaces of two adjacent radiation layers, both assumed to be 0.04 for aluminized films.

2.3. Interlayer Temperature of Composite MLI

The interlayer radiative heat transfer, gaseous conduction, and solid conduction in composite MLI within the liquid hydrogen temperature range are constructed and solved using the layer-by-layer model [23]. Since the heat transfer in composite MLI is one-dimensional, the heat flux between adjacent layers is equal, so that the temperature distribution can calculated via thermal resistance.

The thermal resistance of the SOFI (R_{SOFI}) is given by the following:

$$R_{SOFI} = \frac{L}{\lambda_{SOFI}} \tag{9}$$

The thermal resistance for gaseous conduction (R_g) is given by the following:

$$R_g = \frac{\gamma - 1}{(\gamma + 1)(\frac{R}{8\pi MT})^{\frac{1}{2}} P\alpha} \tag{10}$$

The thermal resistance for radiative heat transfer (R_r) is given by the following:

$$R_r = \frac{(\frac{1}{\varepsilon_i} + \frac{1}{\varepsilon_{i-1}} - 1)}{\sigma(T_i^2 + T_{i-1}^2)(T_i + T_{i-1})} \tag{11}$$

The thermal resistance for solid conduction (R_s) is given by the following:

$$R_s = \frac{\delta}{C_2 f \lambda} \tag{12}$$

Therefore, the total thermal resistance between any two adjacent radiation screen spacer layers in MLI (R_i) is expressed as follows:

$$R_i = R_r + R_s + R_g \tag{13}$$

The heat flux and temperature distribution can be solved using the above equations. Since the heat flux between adjacent layers of MLI is equal, it can be expressed as follows:

$$q_{i-1} = q_i = q_{i+1} \tag{14}$$

The interlayer temperatures in MLI are then solved as follows:

$$T_i = T_C + \frac{\sum_{i=1}^{x} R_i}{\sum_{i=1}^{x} R_i + R_{SOFI}} (T_H - T_C) \tag{15}$$

2.4. Model Validation

To validate the model, the temperature distribution of the composite MLI numerical model is compared with the experimental data from Huang et al. [9], which measured the heat flux and temperature distribution of a composite material consisting of 40 mm SOFI, 42 radiation layers, and 128 spacer layers using a liquid nitrogen evaporation calorimeter system. Table 1 shows the physical properties for composite multilayer adiabatic materials and Figure 2 compares the temperature distribution between the numerical model and the experimental data. Under a vacuum degree of 10^{-3} Pa, with a cold boundary temperature of 77 K and a hot boundary temperature of 293 K, the predicted curve closely matches the experimental data, showing an overall deviation of less than 1.69%.

Table 1. Physical properties for composite multilayer adiabatic materials.

Property	Value
Foam emissivity	0.8
Reflection layer emissivity	0.04
Spacing gas	N_2
Empirical constant of Spacing thermal conductivity	0.008 W/(m·K)

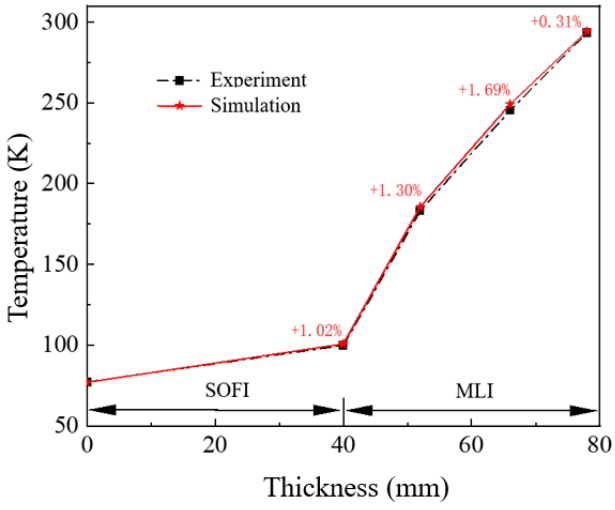

Figure 2. The comparison curve between the model and experimental results.

Additionally, the experimentally measured heat flux through the composite MLI under these conditions is 0.2279 W/m^2, while the heat flux obtained from the numerical model is 0.2298 W/m^2, resulting in an error of 0.83%. The minor discrepancy in heat flux can be attributed to the model's assumption of constant thermal conductivity for the spacer material, whereas in the experiment, the thermal conductivity of the spacer material varies with temperature. Moreover, the vacuum degree might decrease due to outgassing from the MLI, or axial heat leakage of multilayer materials in the experiment may lead to

uneven temperature distribution, thereby affecting the heat flux. Therefore, the established numerical model is suitable for analyzing the heat transfer characteristics of composite MLI.

3. Results and Discussion

3.1. Analysis of Internal Heat Transfer in MLI

To investigate the interlayer temperature distribution in composite MLI within the liquid hydrogen temperature range, simulations were conducted under vacuum conditions of 10^{-3} Pa, with hot boundary temperatures of 273 K and 300 K, respectively. The composite material consisted of 10 mm foam and 30 layers with a density of 28.4 layers/cm. The results are shown in Figure 3. As illustrated in Figure 3a, the temperature variation trends within the composite MLI are consistent for different hot boundary temperatures, gradually increasing along the layer count direction at a cold boundary temperature of 4 K. A significant temperature gradient is observed in the cold boundary region of the composite MLI, which gradually decreases with the layer count and reaches its minimum in the hot boundary region.

Moreover, to reduce the heat flux through the composite MLI, it is essential to analyze the distribution of radiative heat transfer, solid conduction, and gaseous conduction heat fluxes between layers. Figure 3b shows that solid conduction decreases from 0.8324 W/m^2 to 0.2931 W/m^2 along the layer count direction, while radiative heat transfer increases from 0.0244 W/m^2 to 0.4779 W/m^2 under a hot boundary temperature of 300 K. The heat flux exhibits the same trend at a hot boundary temperature of 273 K: radiative heat transfer is not significant near the cold boundary region, and solid conduction dominates. Near the hot boundary region, radiative heat transfer exceeds solid conduction, becoming the dominant heat transfer mechanism. This phenomenon persists even as the hot boundary temperature increases to 300 K. At this point, the thermal insulation performance of the composite MLI can be improved by adding more radiation layers near the hot boundary region or increasing the spacer layers near the cold boundary [24]. Additionally, within the liquid hydrogen temperature range, there exists a critical temperature in the composite MLI where the heat fluxes of radiative heat transfer and solid conduction are equal. As the hot boundary temperature increases from 273 K to 300 K, the critical temperature shifts from point A to point B, indicating that both radiative heat transfer and solid conduction heat fluxes increase in accordance with the rising hot boundary temperature. Furthermore, the increase in radiative heat transfer is more pronounced than that of solid conduction, making radiative heat transfer more sensitive to changes in the hot boundary temperature.

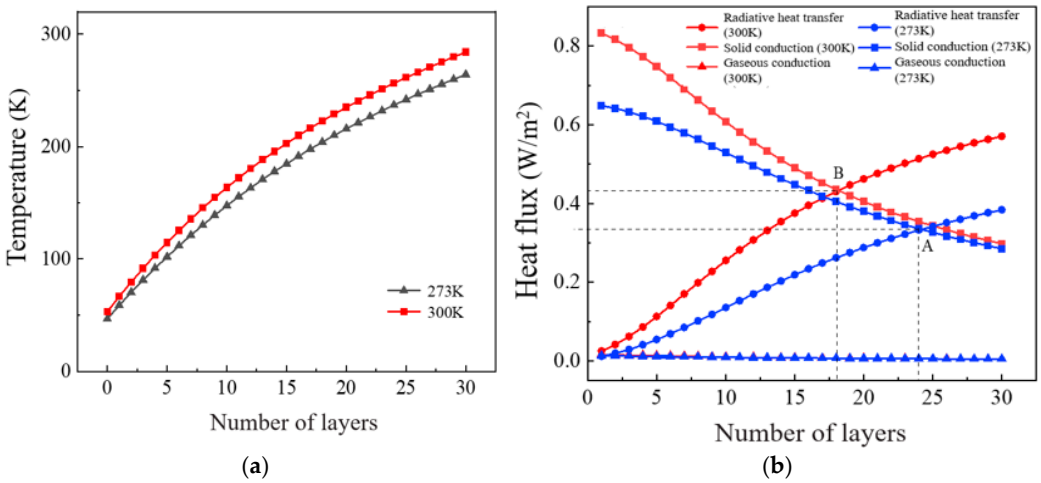

Figure 3. The distribution of temperature and heat flux for different heat transfers in the MLI material: (**a**) temperature distribution; (**b**) distribution of heat transfer rates.

3.2. Impact of Hot Boundary Temperature Variation on Heat Flux

Under vacuum conditions better than 10^{-3} Pa, where gas conduction is negligible, heat transfer through MLI predominantly occurs via interlayer solid conduction and radiative heat transfer between reflective layers. To analyze the variation in these heat transfer mechanisms and the total heat flux with temperature, the heat flux densities of total heat transfer, solid conduction, and radiative transfer are plotted in Figure 4. The figure demonstrates that at a cold boundary temperature of 4 K, the heat flux density through the MLI structure increases as the hot boundary temperature rises. When the cold boundary temperature increases to 20 K, the heat flux follows a similar trend. At a hot boundary temperature of 300 K, the heat flux densities for the two types of MLI are 0.8730 W/m^2 and 0.8100 W/m^2, respectively. The analysis reveals that with increasing hot boundary temperature, the solid conduction, primarily contributed by the interlayer, increases approximately linearly, while the radiative heat transfer through the reflective layers increases at a much higher rate than solid conduction. At low temperatures, the influence of radiative heat transfer is minimal; however, at high temperatures, its impact becomes significant. Furthermore, experimental data indicate that MLI exhibits stable performance at low temperatures, whereas at high temperatures, the radiative heat transfer contributes more significantly to the total heat flux. This understanding is crucial for designing high-performance insulation systems.

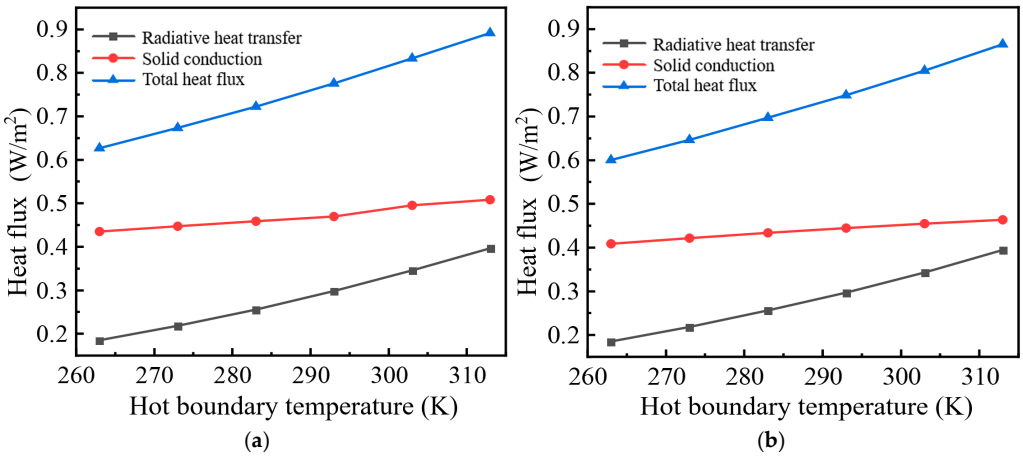

Figure 4. Influence of thermal boundary temperature variation on heat flux in different conductive systems: (**a**) cold boundary temperature of 4 K; (**b**) cold boundary temperature of 20 K.

Additionally, to observe the effects of varying hot boundary temperatures on the three heat transfer components within the liquid hydrogen temperature range, the proportions of solid conduction, radiative heat transfer, and gas conduction at different hot boundary temperatures for the intermediate layer are plotted in Table 2. This illustrates that as the hot boundary temperature increases, the proportion of solid conduction in the total heat flux decreases, while the proportion of radiative heat transfer gradually increases. The proportion of gas conduction decreases only slightly as the hot boundary temperature increases, from 1.08% to 0.87% at a cold boundary temperature of 4 K and from 1.09% to 0.90% at 20 K. When the cold boundary temperature is 20 K and the hot boundary temperature rises from 273 K to 313 K, the proportion of radiative heat transfer increases from 26.38% to 37.48%, while the proportion of solid conduction decreases from 72.52% to 61.61%. At a cold boundary temperature of 4 K, the proportion of radiative heat transfer increases from 32.45% to 44.47%, while the proportion of solid conduction decreases from 66.46% to 54.66%. Therefore, at higher hot boundary temperatures, effectively reducing radiative heat transfer can significantly enhance the insulation performance of the materials, thereby minimizing liquid hydrogen losses within the container.

Table 2. Proportion of three heat transfer modes in composite multilayer insulation materials: (**a**) cold boundary temperature of 4 K; (**b**) cold boundary temperature of 20 K.

(a)			
Hot Boundary Temperature (K)	**Ratio of Heat Flux (%), Cold Boundary Temperature of 4 K**		
	Solid Conduction	**Gaseous Conduction**	**Radiative Heat Transfer**
273	66.46	1.08	32.46
283	63.54	1.03	35.43
293	60.55	0.97	38.48
303	58.55	0.94	40.52
313	54.67	0.87	44.47
(b)			
Hot Boundary Temperature (K)	**Ratio of Heat Flux (%), Cold Boundary Temperature of 20 K**		
	Solid Conduction	**Gaseous Conduction**	**Radiative Heat Transfer**
273	72.53	1.09	26.38
283	69.88	1.05	29.07
293	67.17	1.00	31.83
303	64.40	0.95	34.65
313	61.61	0.90	37.48

3.3. Impact of Foam Insulation Addition Under Different Vacuum Degrees

As the service life increases, actual production and transportation processes will inevitably lead to a decline in the vacuum degree of cryogenic tanks, thereby affecting the insulation performance of composite MLI. Table 3 shows the heat flux through 30 layers of MLI and composite MLI, consisting of 10 mm thick SOFI and 30 layers of MLI within a vacuum range of 10^{-5} Pa to 10^{-1} Pa in the liquid hydrogen temperature range. Under the same hot and cold boundary temperature conditions, the heat flux of the MLI increases from 0.8859 W/m^2 to 0.8959 W/m^2 within the vacuum range of 10^{-5} Pa to 10^{-3} Pa, whereas the heat flux of the composite MLI increases from 0.8655 W/m^2 to 0.8730 W/m^2, with the addition of foam insulation enhancing the insulation performance by only 2.45%. Thus, the addition of foam insulation at high vacuum degrees essentially does not affect the overall thermal insulation performance of the composite MLI. In other words, under these conditions, the MLI primarily governs the reduction in heat flux to the tank, with the foam insulation contributing minimally to the overall insulation performance.

Table 3. Influence of vacuum degree variation on the heat flux of MLI and composite MLI.

Vacuum Degree (Pa)	**Heat Flux (W/m^2)**	
	MLI	**Composite MLI**
10^{-5}	0.8860	0.8655
10^{-4}	0.8871	0.8655
10^{-3}	0.8959	0.8730
10^{-2}	0.9871	0.9420
10^{-1}	1.8980	1.5045

However, as the vacuum deteriorates, the heat leakage in both cases significantly increases. When the vacuum degree rises from 10^{-3} Pa to 10^{-1} Pa, the heat flux of the composite MLI surges from 0.8730 W/m^2 to 1.5045 W/m^2, while for the MLI, the heat flux increases even more, reaching 1.8980 W/m^2. At this point, the addition of foam insulation improves the insulation performance by 20.76%. The vacuum degree significantly impacts the insulation performance of the materials, and the addition of foam

insulation can effectively enhance the insulation performance of composite MLI under low vacuum conditions.

To investigate the effect of vacuum degrees on the internal heat transfer of composite MLI within the liquid hydrogen temperature range, the proportions of the three types of heat transfer under different vacuum conditions are depicted in Figure 5. It can be seen that the proportion of gaseous conduction is less than 1% under vacuum degrees below 10^{-3} Pa. As the vacuum degree increases, the proportion of gaseous conduction gradually rises. When the vacuum degree increases from 10^{-3} Pa to 10^{-1} Pa, the proportion of gaseous conduction sharply increases, accounting for 53.54% of the total heat flux. This is because the number of gas molecules participating in heat transfer is minimal under vacuum degrees better than 10^{-3} Pa, and the internal radiative and solid conduction in the composite MLI are much greater than gaseous conduction, rendering the vacuum effect negligible. However, the deterioration of the vacuum degree leads to a significant increase in the number of gas molecules involved in heat transfer between the MLI layers, thereby increasing the proportion of gaseous conduction and affecting the overall heat flux.

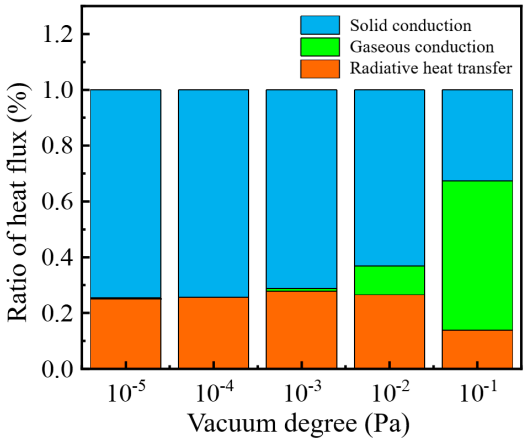

Figure 5. The proportion of three modes of heat transfer under different vacuum conditions.

3.4. Impact of Total Layers of MLI on Heat Flux

The total number of layers in the insulation material significantly influences the interlayer heat transfer in MLI [25]. A common method to reduce heat flux entering storage tanks is by increasing the number of layers of wrapped MLI. Figure 6 shows the heat transfer conditions of composite MLI with different numbers of layers under boundary temperatures of 4 K and 300 K and a vacuum degree of 10^{-3} Pa. To investigate the relationship between solid conduction, radiative heat transfer, and heat flux, the radiative heat transfer and solid conduction heat flux at 1/4, 1/2, and 3/4 positions along the MLI layers are plotted in the figure.

As shown in Figure 6, the total heat flux, solid conduction, and radiative heat transfer through the composite MLI all decrease continuously with the increase in the number of layers, with the rate of heat flux decrease becoming progressively smaller. When the number of layers increases from 40 to 50, the total heat flux decreases by 0.11 W/m^2. However, when the number of layers increases from 50 to 60, the total heat flux decreases by only 0.06 W/m^2. At this point, increasing the number of layers has a negligible impact on enhancing insulation performance, indicating that further increasing the number of layers will not significantly improve performance. Simply increasing the number of layers to enhance the insulation performance of composite MLI is not always effective, as it results in increased tank weight, higher manufacturing complexity, and elevated transportation costs. Therefore, other measures should be considered to improve insulation performance. According to the established model, optimal performance is achieved with 50 layers, resulting in a heat flux of 0.5377 W/m^2 through the composite MLI.

Additionally, analyzing the radiative heat transfer and solid conduction heat fluxes reveals that with the increase in the number of composite MLI layers, radiative heat transfer flux continuously increases, while solid conduction heat flux continuously decreases. At the midpoint of the total number of layers (1/2 position), solid conduction heat flux is greater than radiative heat transfer flux. However, at the 3/4 position of the total number of layers, radiative heat transfer flux surpasses solid conduction heat flux. This indicates that although the total number of layers continues to increase, the critical temperature always exists between the midpoint and the 3/4 position of the total number of layers.

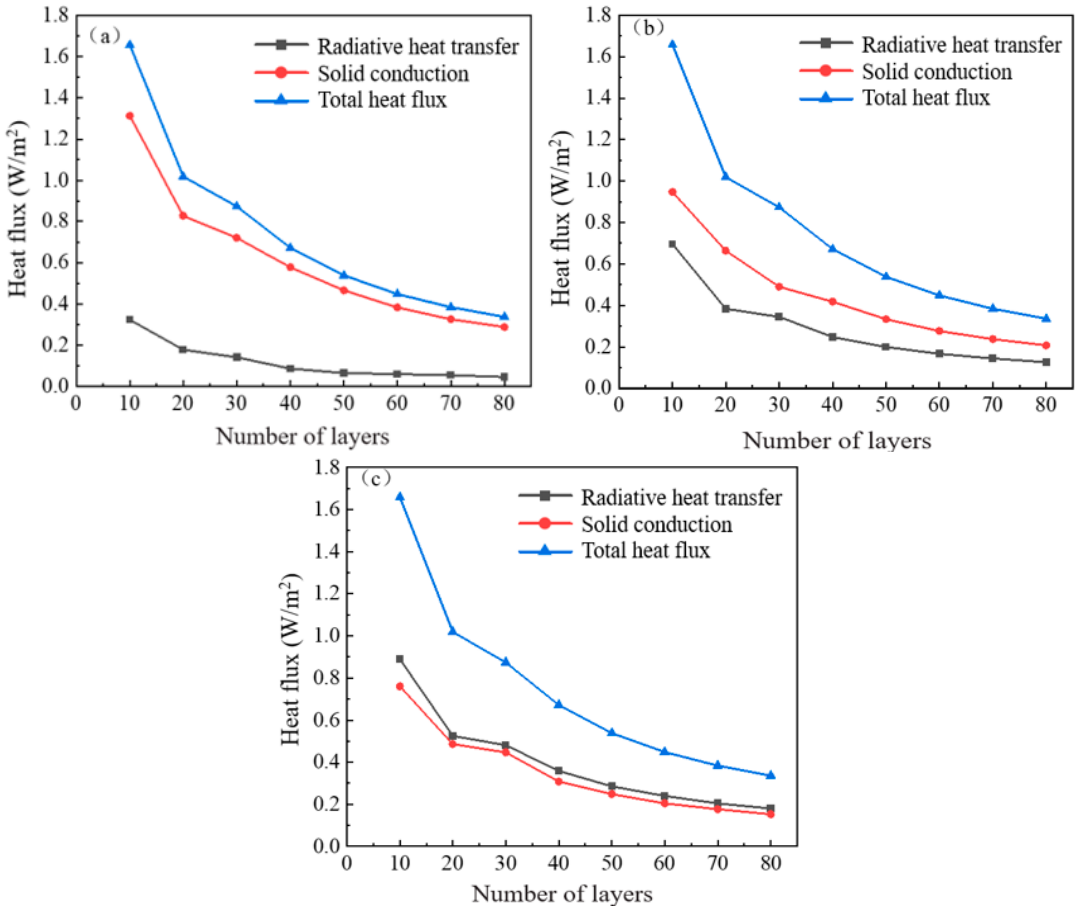

Figure 6. The curve shows the influence of the number of layers on the heat flux: (**a**) heat flux distribution at 1/4 position of MLI material; (**b**) heat flux distribution at 1/2 position of MLI material; (**c**) heat flux distribution at 3/4 position of MLI material.

3.5. Impact of Variable Density on Heat Transfer Characteristics

In accordance with the operational parameters governing the storage and transportation of liquid hydrogen, the inner and outer interlayers of the storage tank are maintained at exceedingly high vacuum levels, thereby placing the MLI in a high vacuum state. In general, radiative heat transfer dominates at high temperatures, while solid conduction is the predominant mechanism at low temperatures. To address the differing heat transfer demands at hot and cold boundaries, researchers have explored variable-density designs based on conventional uniform-density MLI. The key to variable-density design is adjusting the layer density according to the temperature environment. As indicated by previous studies, in low-temperature regions, a looser layer density is required to minimize the impact of solid conduction. In high-temperature regions, an increase in the layer density is necessary in order to enhance the effectiveness of reflective layers in reducing radiative heat transfer. This material combination not only enhances the insulation performance but also reduces the overall mass of the MLI. The implementation of a variable-density design

allows for precise control of MLI performance, ensuring optimal efficiency and stability even in complex scenarios such as liquid hydrogen storage and transportation. This novel design approach offers new directions for the development and application of MLI.

3.5.1. Design of Variable-Density MLI

Currently, researchers categorize variable-density MLI into two-, three-, and four-density regions, based on the differing layer density distributions at low- and high-temperature segments. In practical engineering, implementing four-density regions is challenging due to increased wrapping forces and more complex winding methods. Therefore, variable-density MLI typically employs two-density or three-density regions. As the number of density regions increases, the heat flux density decreases: three-density regions reduce heat flux density by 19.2% compared to two-density regions, while four-density regions further reduce it by 2.4% compared to three-density regions. To minimize the heat flux entering the liquid hydrogen storage tank, this study adopts the three-density region approach for variable-density MLI, combining them with a 10 mm polyurethane foam layer, as illustrated in Figure 7. The goal of using the three-density region design is to optimize composite MLI performance, achieving lower heat flux density while maintaining structural stability, thus enhancing the efficiency and safety of liquid hydrogen storage and transportation.

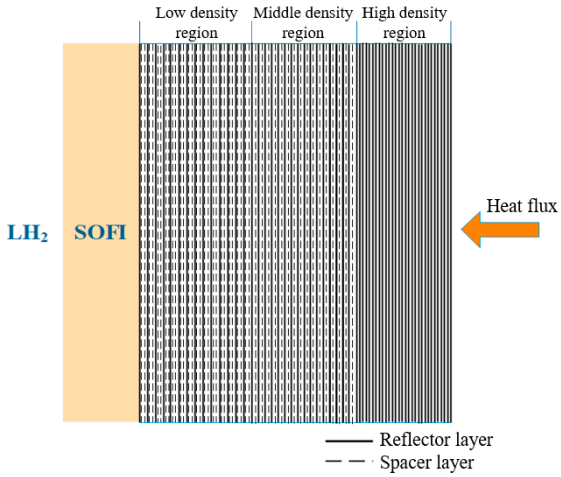

Figure 7. Composite variable-density multilayer insulation structure.

When utilizing a three-density region design, the variable-density MLI is divided into low-density, medium-density, and high-density regions. Typical layer densities are 4 layers/cm, 6 layers/cm, and 8 layers/cm for low-density regions; 10 layers/cm, 12 layers/cm, and 14 layers/cm for medium-density regions; and 16 layers/cm, 18 layers/cm, and 20 layers/cm for high-density regions, as shown in Table 4. The number of layers specifically refers to the reflective layers.

Table 4. Common layer densities of multilayer insulation materials.

Low-Density Region Layer Density (Layer/cm)	Medium-Density Region Layer Density (Layer/cm)	High-Density Region Layer Density (Layer/cm)
8	14	20
6	12	18
4	10	16

Consequently, there are 27 possible combinations of variable-density MLI. To simplify the screening process and summarize the combinations, an orthogonal experimental method was used. In this method, the low-, medium-, and high-density regions are defined as factors A, B, and C, respectively, with different layer densities representing the levels.

By selecting three levels for each factor, a three-factor, three-level orthogonal experimental model is constructed to facilitate the summarization and screening process. The factors and levels are detailed in Table 5. This design aids with systematically examining the influence of various factors and levels on insulation performance, thereby identifying the optimal layer density combination. In this setup, the total thickness of the variable-density MLI is 30 mm, and the SOFI thickness is 10 mm. With a hot boundary temperature of 300 K, numerical calculations of the heat flux density under identical conditions for the respective combinations were performed to determine the optimal combination. This provides a basis for subsequent studies on interlayer temperature and component evaporation under variable-density combinations.

The results of heat flux density calculations for different layer density combinations are shown in Table 6. The optimal combination for composite variable-density MLI is A1B1C1, where the low-density region has a layer density of 8 layers/cm, the medium-density region has 14 layers/cm, and the high-density region has 20 layers/cm. With this layer density configuration, the minimum heat flux density through a 30 mm-thick MLI material is achieved, reaching 0.4480 W/m^2. This approach utilizes the orthogonal experimental method to determine the optimal combination of commonly used layer densities when applied to the insulation of liquid hydrogen storage tanks. It enables a reasonable allocation of reflective layers in low-, medium-, and high-density regions when determining the thickness of the insulation layer, thus saving time in the variable-density allocation for liquid hydrogen storage tanks.

Table 5. Factors and levels of layer density in multilayer insulation materials.

Levels	Factor A	Factor B	Factor C
	Layer Density of Low-Density Region (Layer/cm)	Layer Density of Medium-Density Region (Layer/cm)	Layer Density of High-Density Region (Layer/cm)
1	8	14	20
2	6	12	18
3	4	10	16

Table 6. Results and analysis of density variation and heat flux at the cold boundary temperature of 4 K liquid hydrogen storage tanks.

Case Numbers	Factors			VD-MLI Heat Leakage (W/m^2)
	A	B	C	
1	1	1	1	0.4480
2	1	2	2	0.4576
3	1	3	3	0.4688
4	2	1	2	0.4800
5	2	2	3	0.4928
6	2	3	1	0.4912
7	3	1	3	0.5104
8	3	2	1	0.5200
9	3	3	2	0.5232
K1	0.4581	0.4794	0.4864	
K2	0.4880	0.4901	0.4869	
K3	0.5178	0.4944	0.4906	
R	0.0597	0.0149	0.0042	

K1, K2, and K3 represent the mean values for factors A, B, and C, respectively; R denotes the range for each factor.

Furthermore, heat flux density varies with different combinations of layer densities and changes in the configuration of reflective and spacer layers in the radial direction. The density variation in the low-density region significantly affects the overall heat flux density. Analysis of different variable-density MLI structures reveals that a significant difference in

the density of reflective screens in different density regions results in enhanced insulation performance. However, in actual manufacturing processes, the layer density in the cold boundary region should not be too low, to prevent issues such as the detachment of reflective layers. Therefore, within the constraints of the manufacturing process, optimizing the composite MLI structure by appropriately adjusting layer density can enhance insulation performance. This ensures improved tank insulation performance while avoiding potential manufacturing issues.

3.5.2. Influence of Variable Density on Interlayer Temperature Distribution

To study the relationship between variable density and temperature distribution, we selected the optimal layer density from Section 3.5.1 and conducted a comparative analysis with the corresponding uniform density. We performed a computational analysis of various composite MLI structures at a hot boundary temperature of 300 K for a liquid hydrogen storage tank. Figure 8 illustrates the temperature distribution for different layer density MLI structures.

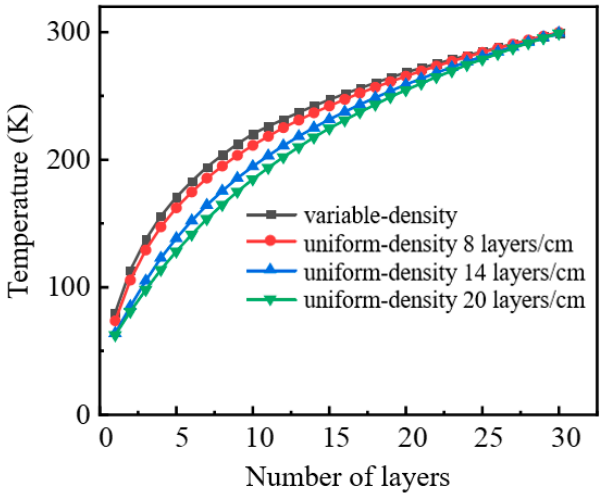

Figure 8. Temperature distribution chart of different layer densities.

As shown in the figure, both variable-density and uniform-density MLI exhibit similar upward trends. For uniform-density MLI, as the layer density decreases, the temperature increase near the cold boundary becomes more pronounced, while it becomes more gradual near the hot boundary. In contrast, the variable-density MLI demonstrates a greater temperature variation, with the temperature rise near the cold boundary even surpassing that of the insulation material composed solely of the lowest layer density in the variable-density arrangement. Furthermore, as the layer density decreases from 20 layers/cm to 8 layers/cm, the interlayer temperature between the SOFI and MLI in the composite uniform-density material increases from 62.65 K to 73.62 K. This indicates that the interlayer temperature decreases as the layer density increases. When the layer density decreases from 20 layers/cm to 14 layers/cm, the interlayer temperature increases by only 1.45 K. However, when the layer density decreases from 14 layers/cm to 8 layers/cm, the interlayer temperature increases by 9.58 K. This suggests that reducing the layer density can enhance the performance of the MLI material, but the improvement in insulation performance becomes less significant with further reduction in layer density.

3.5.3. Effect of Variable Density on Heat Leakage

Figure 9 visually compares the heat flux density of variable-density and uniform-density MLI structures. As illustrated in Figures 4–10, the heat flux density of uniform density of MLI continuously decreases as layer density decreases, reaching a minimum of 0.4201 W/m^2 at a layer density of eight layers/cm. The heat flux density for variable-

density structures shows significant differences compared to various uniform-density structures. Compared to a uniform density of 20 layers/cm, the heat flux density decreases by 0.1680 W/m^2 in the variable-density structure; however, compared to a uniform density of eight layers/cm, the heat flux density increases by 0.028 W/m^2. The phenomenon is primarily because, in an eight layers/cm uniform-density MLI material, the spacers in the variable-density structure have significantly less mass than those in the uniform-density structure, leading to substantial differences in insulation performance. These differences are not of the same order of magnitude. Therefore, comparing variable-density with uniform-density MLI requires considering the spacer layer thickness and the number of layers under different structures. When these conditions are met, a uniform density of 14 layers/cm can be used for comparison. In this case, the variable-density MLI material reduces the heat flux density by 0.0607 W/m^2, representing a 13.5% improvement in insulation performance compared with the uniform-density material at the same level.

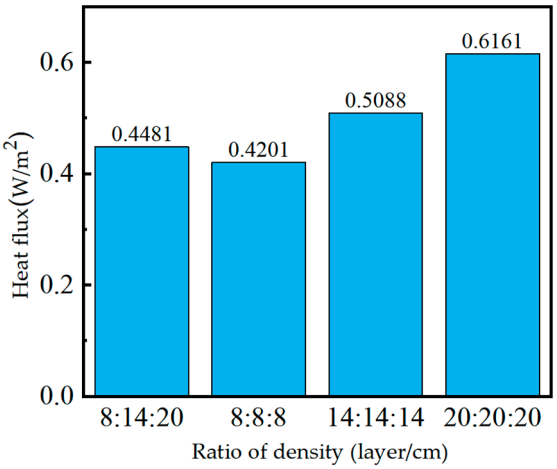

Figure 9. Comparison of heat flux density for different layer densities.

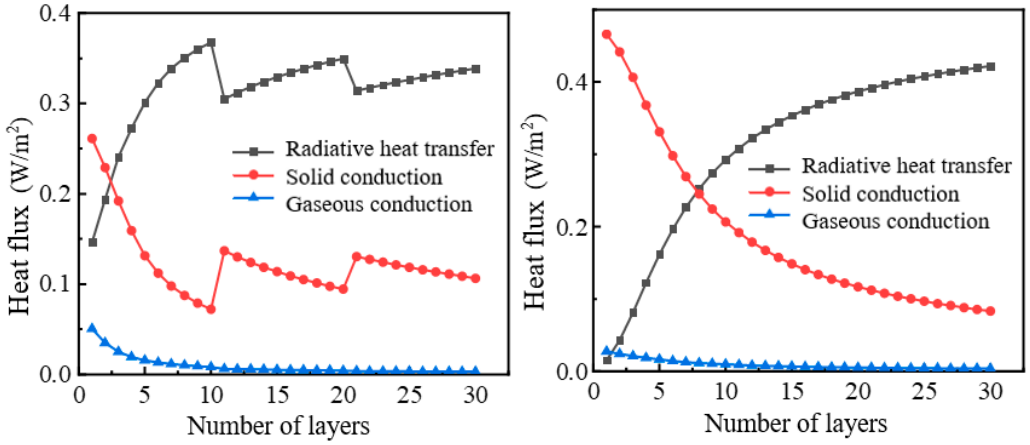

Figure 10. The heat flux distribution of three items of the composite MLI material.

To explore the impact of variable density on heat flux density, Figure 10 plots the heat flux of three components in the composite structure within a layer density of 14 layers/cm. The figure shows that, for variable-density MLI, the gas thermal conductivity changes little along the thick direction of the insulation layer (i.e., the direction of increasing temperature), while solid thermal conductivity decreases and radiative heat transfer increases. Additionally, two significant increases in solid thermal conductivity and two noticeable decreases in radiative heat transfer are observed. These changes mainly occur at the transition points from low-density to medium-density and from medium-density to high-density regions.

This is primarily due to an increase in the number of reflective layers and the reduction in the number of spacer layers.

3.5.4. Impact of Variable Density on Component Evaporation

To further investigate the impact of variable-density composite MLI on the hydrogen storage capacity, the heat leakage and internal component evaporation for a layer density ratio of 8:14:20 compared to a uniform density of 14 layers/cm are depicted in Table 7. As shown in the table, both heat leakage and component evaporation are significantly reduced in the variable-density MLI compared to the uniform-density MLI under identical conditions. This indicates that the insulation performance of variable-density MLI is superior to that of uniform-density MLI with the same thickness.

Table 7. Influence of variable-density structure on the evaporation rate of liquid hydrogen tanks.

Structure	Heat Leakage (W)	Component Evaporation (%/d)
Variable density Layer density ratio: 8:14:20	0.0695	0.0385
Uniform density Layer density ratio: 14:14:14	0.0789	0.0437

Considering economic efficiency, it is also essential to comprehensively evaluate the composite material structure. The economic analysis should account for factors such as the mass, material type, and cost of the composite variable-density material structure. Table 8 summarizes a comparison of the mass between uniform-density and variable-density MLI.

Table 8. Comparison of density structure quality.

Parameter of Materials	Uniform Density	Variable Density		
		Low-Density Region	Medium-Density Region	High-Density Region
Thickness (mm)	30	10	10	10
Layer density (layer/cm)	14	8	14	20
Matching scheme (reflector + spacer layer)	1 + 4	1 + 6	1 + 4	1 + 2
Alu-layers (layers)	$3 \times 14 = 42$	$8 + 14 + 20 = 42$		
Poly-layers (layers)	$42 \times 4 = 168$	$8 \times 6 + 14 \times 4 + 20 \times 2 = 144$		
Alu-layer weight (kg)	0.0044	0.0044		
Poly-layer weight (kg)	0.00635	0.00635		
Total mass per unit (kg)	1.2516	1.0992		
SOFI weight (kg)	$0.46\delta_{SOFI}$	$0.46\delta_{SOFI}$		
Total mass reduction (%)		$(1.2516 - 1.0992)/1.2516 = 12.18\%$		

As shown in the table, the mass of the composite variable-density MLI increases with the thickness of both the foam layer and the variable-density MLI layers. However, the impact on the mass of the composite variable-density MLI differs between the foam layer thickness and the variable-density MLI thickness. Specifically, increasing the foam layer thickness has a more pronounced effect on the mass of the composite variable-density MLI, while the impact of increasing the variable-density MLI thickness is relatively smaller. Therefore, in practical engineering applications, reducing the foam layer thickness is more effective in decreasing the mass of the composite variable-density MLI than reducing the variable-density MLI thickness, while still meeting heat leakage requirements. This approach further enhances the economic viability of the composite variable-density MLI. Additionally, compared to uniform-density MLI, the overall mass of variable-density MLI is reduced by 12.8%, significantly contributing to improved economic efficiency. When designing and selecting composite variable-density MLI, it is crucial to consider not only

their thermal insulation performance but also their economic factors. By optimizing the thickness of the foam layer and the variable-density MLI, material costs can be reduced while ensuring effective insulation, thereby achieving a more efficient and cost-effective solution for liquid hydrogen storage and transportation.

3.6. Optimization Study on Heat Transfer Characteristics of Structural Parameters

In practical production, the structural parameters of composite variable-density MLI are not confined to a single element. Altering one element often leads to compromises due to external factors like spacer thickness, causing fluctuations in the values of other elements. Therefore, it is imperative to study how to achieve optimal insulation performance within limited spatial constraints.

To investigate the optimal insulation performance under varying foam thickness, number of insulation layers, and variable-density conditions, an orthogonal experimental design method with three factors and three levels is employed. Factor A represents SOFI thickness (10 mm, 20 mm, 30 mm), Factor B represents the number of insulation layers (30, 40, 50), and Factor C represents the density ratio of the MLI (8:14:20, 14:14:14, 6:12:18). The factors and levels are listed in Table 9. Numerical calculations of heat flux density under different combinations are performed to determine the relationship between each parameter and the insulation performance of the composite variable-density MLI.

Table 9. Factors and levels.

Levels	Factor A	Factor B	Factor C
	Thickness of SOFIs (mm)	Number of Layers of MLI	Ratio of Density
1	10	30	8:14:20
2	20	40	14:14:14
3	30	50	6:12:18

The calculated heat flux densities for different structural parameter combinations are shown in Table 10. The table indicates that the optimal combination for minimizing heat flux density in the composite variable-density MLI includes a foam thickness of 10 mm, 50 insulation layers, and a density ratio of 8:14:20. With this optimal combination, the minimum heat flux density achieved is 0.3024 W/m^2. This orthogonal experimental method offers an allocation method for structural parameters in the insulation of liquid hydrogen tanks. Given that the order of significance is $R_B > R_C > R_A$, when the interlayer space of the storage tank is fixed, the number of insulation layers should be prioritized, followed by the adjustment of variable density in the composite MLI, and finally the determination of the foam layer thickness.

Table 10. Calculation results of heat flux density under different structural parameters.

Case Numbers	Factors			VD-MLI Heat Leakage (W/m^2)
	A	B	C	
1	1	1	1	0.4480
2	1	2	2	0.4000
3	1	3	1	0.3024
4	2	1	2	0.5440
5	2	2	3	0.3680
6	2	3	1	0.3029
7	3	1	3	0.4864
8	3	2	1	0.3615
9	3	3	2	0.3224
K1	0.3787	0.4928	0.3705	
K2	0.4046	0.3765	0.4221	
K3	0.3901	0.3042	0.3808	
R	0.0259	0.1886	0.0516	

K1, K2, and K3 represent the mean values for factors A, B, and C, respectively; R denotes the range for each factor.

4. Conclusions

A numerical model based on the layer-by-layer approach, considering radiation, solid, and thermal conduction in the liquid hydrogen temperature range is proposed to study the heat transfer behavior of composite MLI. The following conclusions were drawn from this study:

(1) A novel method, incorporating an accuracy model, was developed to gain insight into the heat transfer characteristics of composite MLI within the liquid hydrogen temperature range. This study examined the steady-state interlayer temperature distribution and the variation in heat flux per unit area with respect to the hot boundary temperature, while also exploring the effects of vacuum level and total number of MLI layers on insulation performance.

(2) Gas conduction is insignificant in high vacuum heat transfer processes, accounting for less than 1%. Radiative heat transfer dominates near the hot boundary, while solid conduction dominates near the cold boundary. Within the MLI, there exists a critical temperature where radiative and solid conduction heat transfer are equal. This temperature rises with increasing hot boundary temperature and shifts towards the cold boundary, consistently lying between the 1/2 and 3/4 positions of the total number of MLI layers.

(3) Under vacuum conditions better than 10^{-3} Pa, the MLI dominates heat transfer suppression, with SOFI having minimal impact on the overall insulation performance, enhancing it by only 2.45%. When the vacuum degree deteriorates from 10^{-3} Pa to 10^{-1} Pa, the increase in gas molecule density causes the heat flux to jump from 0.8730 W/m^2 to 1.3665 W/m^2. Under these conditions, the composite MLI improves insulation performance by 20.76% compared to the MLI alone.

(4) Increasing the total number of MLI layers enhances the insulation performance of composite MLI. Considering both performance and cost, an optimal insulation effect is achieved with 50 layers, resulting in a heat flux of 0.5377 W/m^2.

Author Contributions: Conceptualization, M.Y. and L.J.; methodology, Y.W.; software, S.J.; formal analysis, M.Y.; resources, D.S.; data curation, Y.D.; writing—original draft preparation, Y.D.; writing—review and editing, L.J. All authors have read and agreed to the published version of the manuscript.

Funding: This research was funded by the Key Research and Development Project of Jiangsu Province (BE2022001-5); the Science and Technology Project of State Administration for Market Regulation (2023MK041); the Science and Technology Project of Jiangsu Province Market Supervision Administration (KJ2023001); the Junior Science and Technology Project of Special Equipment Safety Supervision Inspection Institute of Jiangsu Province (KY(YJ)2023007); the Open-sharing and Independent Research Project for Large-scale Scientific Instruments of Jiangsu Province (TC2023A062); and the Jiangsu Provincial Double-Innovation Doctor Program (JSSCBS20230188).

Institutional Review Board Statement: Not applicable.

Informed Consent Statement: Informed consent was obtained from all subjects involved in the study.

Data Availability Statement: Data are contained within the article.

Conflicts of Interest: The authors declare no conflict of interest.

Nomenclature

C_2	Constant
C_p	Specific heat at constant pressure (kJ/(kg·K))
C_v	Specific heat at constant volume (kJ/(kg·K))
f	Relative density (-)
L	Thickness (m)
P	Vacuum degree (Pa)
q	Heat flux (W/m^2)
R	Thermal resistance (K/W))

T	Temperature (K)
Greek letters	
α	Thermal accommodation coefficient (-)
λ	Thermal conductivity (W/(m·K))
γ	Ratio of C_p and C_v (-)
δ	Thickness of the spacer layer (m)
σ	Stefan–Boltzmann constant ($W/m^2 \cdot K^4$)
ε	Emissivity (-)
Abbreviation	
MLI	Multilayer insulation
SOFI	Spray-on foam insulation
Subscripts	
1,. . .i	Layer number
C	Cold
g	Gaseous conduction
H	Hot
r	Radiative heat transfer
S	SOFI
s	Solid conduction
tot	Total

References

1. Jiang, L.; Xie, R.Y.; Shi, W.K.; Wu, E.Y.; Li, B.; Zhang, X.J. Water effect on adsorption carbon capture in metal-organic framework: A molecular simulation. *Carbon Capture Sci. Technol.* **2022**, *4*, 100061. [CrossRef]
2. Shi, W.K.; Ji, Y.; Zhang, X.J.; Fang, M.X.; Wang, T.; Jiang, L. Understandings on design and application for direct air capture: From advanced sorbents to thermal cycles. *Carbon Capture Sci. Technol.* **2023**, *7*, 100114. [CrossRef]
3. Hájková, P.; Horník, J.; Čižmárová, E.; Kalianko, F. Metallic Materials for Hydrogen Storage—A Brief Overview. *Coatings* **2022**, *12*, 1813. [CrossRef]
4. Naquash, A.; Agarwal, N.; Lee, M. A Review on Liquid Hydrogen Storage: Current Status, Challenges and Future Directions. *Sustainability* **2024**, *16*, 8270. [CrossRef]
5. Xie, F.; Xia, S.; Zhu, Y.; Ma, Y.; Wang, L.; Li, Y. Development of small hydrogen liquefaction device based on G-M refrigerator. *Cryogenics* **2022**, *2*, 1–6.
6. Hu, W.; Shen, L.; Peng, X.; Yu, H. Key technology analysis of boil-off control study on cryogenic propellant long-term application on orbit. *Cryogenics* **2011**, *3*, 59–66.
7. Davide, C.; Carmela, C.; Giordano, E.S.; Robert, E.; Frank, O.; Valerio, C. Analysis of High Temperature Degradation of Multi-layer Insulation (MLI) Systems for Liquid Hydrogen Storage Tanks. *Chem. Eng. Trans.* **2023**, *99*, 415–420.
8. Hastings, L.J.; Martin, J.J. Experimental testing of a foam MLI (FMLI) thermal control system (TCS) for use on a cryogenic upper stage. *AIP Conf. Proc.* **1998**, *420*, 331–341.
9. Huang, C.; Zhang, Y. Calculation of high-temperature insulation parameters and heat transfer behaviors of MLI by inverse problems method. *Chin. J. Aeronaut.* **2014**, *27*, 791–796. [CrossRef]
10. Li, K.; Chen, J.; Tian, X.; He, Y. Study on the Performance of Variable Density Multilayer Insulation in Liquid Hydrogen Temperature Region. *Energies* **2022**, *15*, 9267. [CrossRef]
11. Maynard, N.; Louriou, C.; Estebe, B. Model Based Exploration of Physical Parameters for Liquid Hydrogen System Insulation Performance. *IOP Conf. Ser. Mater. Sci. Eng.* **2024**, *1301*, 012067. [CrossRef]
12. Jiang, Y.; Zhang, P.; Sun, P.; Li, P. Thermal insulation properties of composite multilayer thermal s under atmospheric condition. *Cryog. Supercond.* **2020**, *48*, 1–6.
13. Hastings, L.; Hedayat, A.; Brown, T. *Analytical Modeling and Test Correlation of Variable Density MLI for Cryogenic Storage*; NASA: Washington, DC, USA, 2004.
14. Xie, T.; He, Y.-L.; Tong, Z.-X. Analysis of insulation performance of multilayer thermal insulation doped with phase change material. *Int. J. Heat Mass Transf.* **2016**, *102*, 934–943. [CrossRef]
15. Liu, Z.; Li, Y.; Xie, F.; Zhou, K. Thermal performance of foam/MLI for cryogenic liquid hydrogen tank during the ascent and on orbit period. *Appl. Therm. Eng.* **2016**, *98*, 430–439. [CrossRef]
16. Johnson, W.; Demko, J.A.; Fesmire, J. Analysis and testing of multilayer and aerogel insulation configurations. *AIP Conf. Proc.* **2010**, *1218*, 780–787.
17. Lv, H.; Zhang, Z.; Chen, L.; Zhang, Z.; Chen, S.; Hou, Y. Thermodynamic analysis of vapor-cooled shield with para-to-ortho hydrogen conversion in composite multilayer insulation structure for liquid hydrogen tank. *Int. J. Hydrogen Energy* **2024**, *50*, 1448–1462. [CrossRef]
18. Kang, D.H.; An, J.H.; Lee, C.J. Numerical modeling and optimization of thermal insulation for liquid hydrogen storage tanks. *Energy* **2024**, *291*, 130143. [CrossRef]

19. Wang, B.; Wang, H.; Gao, Y.; Yu, J.; He, Y.; Xiong, Z.; Lu, H.; Pan, Q.; Gan, Z. Theoretical analysis of entropy generation in multilayer insulations: A case study of performance optimization of variable density multilayer insulations for liquid hydrogen storage systems. *Int. J. Hydrogen Energy* **2024**, *85*, 175–190. [CrossRef]
20. Li, F. Study on the Insulation Performance of Composite MLI. Master's Thesis, Zhejiang University, Hangzhou, China, 2017.
21. Barrios, M.; Vanderlaan, M.; Van Sciver, S. Thermal conductivity of spray-on foam insulations for aerospace applications. *AIP Conf. Proc.* **2012**, *1434*, 1319–1326.
22. Tien, C.; Cunnington, G. Cryogenic insulation heat transfer. *Adv. Heat Transf.* **1973**, *9*, 349–417.
23. Li, Y.; Deng, Y.; Kuang, C.; Xu, J.; Zhang, Y. Analysis and Research on High Vacuum MLI Heat Transfer Calculation Model for LNG Storage Tanks. *Sci. Technol. Innov.* **2021**, *11*, 12–14.
24. Xu, X.; Chen, L.; Zheng, J.; Wang, J. Study on the Heat Leakage Characteristics of Spacecraft Variable Density Multilayer under Variable Operating Conditions. *Vac. Cryog.* **2020**, *26*, 295–300.
25. Shu, Q.; Fast, R.; Hart, H. Heat flux from 277 to 77 K through a few layers of MLI. *Cryogenics* **1986**, *26*, 671–677. [CrossRef]